0254-6124/2026/46(5)-0001-11 *Chin. J. Space Sci.* 空间科学学报

HU Yuanqiao, LIU Wenlong, YAN Li, ZHANG Dianjun, HE Bin. Statistical Study of Plasmaspheric Plumes Based on THEMIS Observations. *Chinese Journal of Space Science*, 2026, **46**(5): 1–11. CSTR:32142.14.cjss.2025–0240. DOI:10.11728/cjss2026.05.2025–0240

Statistical Study of Plasmaspheric Plumes Based on THEMIS Observations*

HU Yuanqiao LIU Wenlong YAN Li

ZHANG Dianjun HE Bin

1(*School of Space and Earth Science*, *Beihang University*, *Beijing* 102206)

2(*Key Laboratory of Space Environment Monitoring and Information Processing of MIIT*, *Beihang University*, *Beijing* 102206)

Abstract A comprehensive statistical study of detached plasmaspheric plumes is presented, based on THEMIS observations from 2011 to 2022. Using electron densities derived from spacecraft potential measurements, we identify 488 detached plume crossings and investigate their spatial distribution, density characteristics, and morphological properties across the magnetosphere. The results show that plasmaspheric plumes occur primarily within L = 5 – 8.5, with the highest occurrence near L = 6 – 6.5. Additionally, plumes exhibit a pronounced dawn-dusk asymmetry, with significantly more events observed in the dusk sector than in the dawn sector, a trend that remains consistent even after accounting for the effects of orbital sampling, with the duskside showing the highest occurrence rate of plume crossings. In contrast, plumes observed on the dayside tend to extend to larger L than those in other Magnetic Local Time (MLT) sectors, reflecting the sunward wrapping of the entire plume structure as it extends from the duskside toward the dayside. The electron densities of plumes are typically concentrated in the range of 60 – 90 cm^{-3}. Plume densities decrease outward from L = 5 – 6, indicating that plume plasma becomes progressively diluted as it extends outward. Density gradients within plumes are also quantified for the first time in a statistical sense. Both positive density gradients (G_{pos}) and negative density gradients (G_{neg}) generally decrease with increasing L and show clear dawn–dusk asymmetry, with stronger gradients on the dawnside and weaker gradients on the duskside for L > 6. Morphologically, most plumes have radial widths of ΔL = 0.2 – 1.0, and plumes on the duskside exhibit larger ΔL than those in other MLT sectors. In addition, plume electron density increases with ΔL, suggesting that plumes with smaller ΔL are accompanied by a faster reduction in electron density. These results provide a comprehensive statistical framework for understanding plume formation, evolution, and their potential roles in magnetospheric dynamics.

Key words Plasmasphere, Plasmaspheric plume, Spatial characteristics, Electron density gradients

Classified index P353

0 Introduction

The Earth's plasmasphere, a corotating, torus-shaped region of cold (< 10 eV) and dense (10 – 10^4 cm^{-3}) plasma, is an important component of the inner magnetosphere[1–10]. It is the extension of the ionosphere, providing plasmasphere filling with ionospheric ions and electrons trapped on closed geomagnetic field lines[11–15]. The outer boundary of the plasmasphere, the plasmapause, is dominated by the balance between convection

* Supported by National Natural Science Foundation of China (42441809)
Received December 29, 2025. Revised April 19, 2026

©The Author(s) 2026. This is an open access article under the CC-BY 4.0 License (https://creativecommons.org/licenses/by/4.0/)

electric field and corotation electric field. At the plasmapause, plasma density decreases sharply as field lines transition from closed drift paths to open convective trajectories[16,17].

The plasmaspheric plume is a stretch of the outer region of the plasmasphere and is recognized as a dynamic feature of this region[18–21]. When the magnetospheric convection electric field intensifies, the outer plasmasphere is eroded, leading to a contraction of the main plasmasphere. This erosion transports cold, dense plasma outward and sunward, resulting in the formation of plasmaspheric plumes[22–24].

Plasmaspheric plumes play important roles in the magnetosphere, such as wave generation[25–30], wave-particle interactions[31,32], particle precipitation[33–35], and the dayside magnetic reconnection[6,36–38]. For instance, Zhou *et al.*[35] demonstrate that significant plasma density variations near the edge of the plumes could be one of the major mechanisms that drive the dispersed precipitation events in the dusk and postnoon sectors. Therefore, characterizing the spatial structure and temporal evolution of plumes is essential.

The dynamics and morphology of plasmaspheric plumes have been investigated using *in-situ* satellite observations[6,39–43], remote sensing from the Extreme Ultraviolet (EUV) images[3,4,44–46] and ground-based instruments[47,48]. Although EUV images provide global views of plume morphology[8,49], its limited sensitivity to low-density plasma makes it difficult to resolve plumes at high L. Therefore, *in-situ* satellite measurements are employed in this study to characterize plume structures and properties.

Observations of plasmaspheric plumes at different locations in the magnetosphere have been made using various spacecraft[6,40–43,50,51]. For example, Cluster observations revealed that most of the plumes in the outer magnetosphere have ΔL below 1.5. Besides, plumes at lower L are observed in all MLT sectors, whereas those at higher L appear only in the afternoon sector[40,43]. Borovsky and Denton[52] found that plumes at geosynchronous orbit can persist for several days, with both ΔL and the plasma density tend to decrease with the plume age. Using density data from the THEMIS spacecraft, Walsh *et al.*[6] showed that plumes at the magnetopause are present 12.5% of the crossings and electron densities of plumes can be as large as 300 cm^{-3}. Previous studies consistently showed that plumes are more often found in the dusk sector[40–43,51]. However, no comprehensive study has characterized plume properties across the entire magnetosphere, particularly their electron density and electron density gradients.

In this study, we utilize extensive measurements from the THEMIS spacecraft to statistically investigate the spatial distribution, densities, and morphological properties of plasmaspheric plumes across the magnetosphere, including the first systematic analysis of plume density gradients.

1 Data and Method

1.1 Data

The dataset used in this study is obtained from the THEMIS mission. The THEMIS mission[53] comprises five satellites, launched on 17 February 2007, each possessing an orbital inclination of approximately 11° with perigees of ~ 1.5 R_e and apogees of ~ 12 R_e. After THEMIS-B and THEMIS-C commenced lunar orbit insertion maneuvers on 20 July 2009, THEMIS-A, THEMIS-D, and THEMIS-E were still in their orbits to observe the Earth's magnetosphere. The spacecraft pass through the plasmapause twice in each orbit period of about one day and cover all MLT sectors of the inner magnetosphere approximately once per year. THEMIS-D and THEMIS-E are operated in close trajectories and are likely to observe the same plume structure. Therefore, we selectively utilize datasets from THEMIS-A and THEMIS-E.

We use the spacecraft potential measurements from the Electric Field Instrument (EFI)[54], as well as ion and electron measurements from the Electrostatic Analyzer (ESA)[55]. Since the cold plasmaspheric plasma is primarily below the lower energy threshold of ESA (~ 5 eV), the electron densities must be inferred from the spacecraft potential and electron thermal velocity measured by the EFI and ESA instruments, respectively[56–59].

1.2 Identification of the Plume Events

Figure 1 illustrates a representative plasmaspheric plume crossing event observed by THEMIS-A on 29 December 2011. Figure 1(a) shows the spacecraft potential

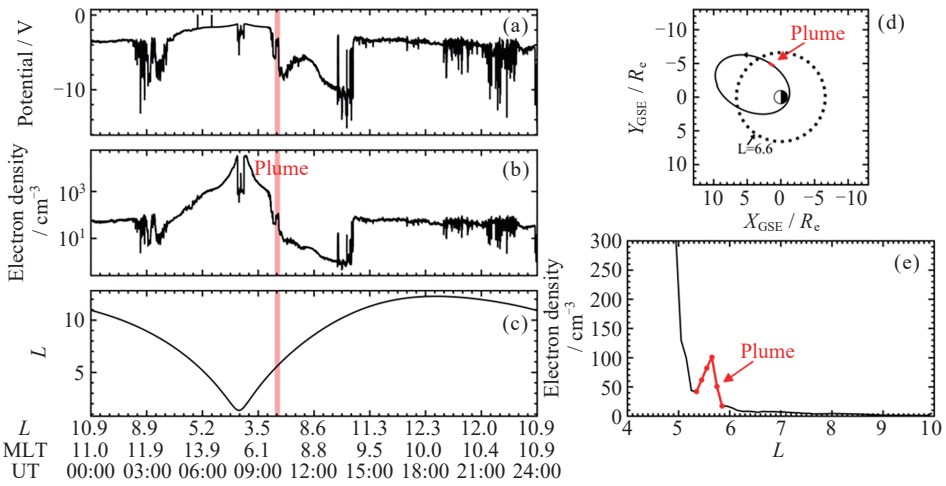


Fig. 1 Example of plasmaspheric plume observed by THEMIS-A spacecraft on 29 December 2011 in GSE coordinates. (a) Spacecraft potential measured by EFI instrument. (b) Electron density derived from spacecraft potential. (c) L. (d) Spacecraft trajectory. The solid red line represents orbit during the plume. (e) Electron density as a function of L. The red line and dots represent the plume. The red shadows in (a) –(c) indicate the time interval of the detected plasmaspheric plume

measured by EFI. The electron density derived from the spacecraft potential is plotted in Figure 1(b). At 09:53 UT, the electron density increases from 42.1 to 100.8 cm^{-3} following a sharp decrease near 09:40 UT which indicates the plasmapause crossing. This enhancement, highlighted by the red shading in Figures 1(a) –(c), suggests a detached plume structure. The spacecraft trajectory in Geocentric Solar Ecliptic (GSE) coordinates is shown in Figure 1(d), with the red segment denoting the portion of the orbit during which the plume was encountered.

To examine the spatial variation of this event, the electron density is binned as a function of L from L = 4 to 10, with a bin width of 0.1. The variation of electron density with L is derived for each inbound or outbound crossing, with the result for the outbound crossing illustrated in Figure 1(e). As THEMIS-A moves outward across the plasmapause, the electron density sharply decreases to a minimum of 42.1 cm^{-3} at L = 5.3. After that, it increases to a peak of 100.8 cm^{-3} at L = 5.6, and finally decreases to a low value of 17.5 cm^{-3} at L = 5.8. This characteristic profile provides clear evidence for a plasmaspheric plume detached from the main plasmasphere[60].

In this study, plasmaspheric plumes are identified based on the following criteria. (i) We identify a plasmapause crossing if the electron density changes by a factor $\geqslant$ 5 within 0.5 L. Such a criterion has been widely used in previous studies[7,16,20]. (ii) If the spacecraft is located outside the plasmapause and the electron density typically decreases to a value below 50 cm^{-3} with increasing L, then rises to a value above 70 cm^{-3} and subsequently decreases again, the structure is identified as a plasmaspheric plume. (iii) ΔL is defined as difference between the L of the entrance and exit of the plume. Referencing the criterion of plasmaspheric plume identification by Darrouzet *et al.*[43] and Zhang *et al.*[61], we consider that the case with $0.2 < \Delta L < 2$ can be identified as a plasmaspheric plume by satellite. (iv) Events occurring in the magnetosheath are excluded, since transient density enhancements in this region may arise from magnetosheath turbulence rather than actual plume structures. (v) The lower threshold for plume identification is set based on the plasmaspheric density model given in Eq. (1) by Sheeley *et al.*[60].

$$n_e = 10 \times \left(\frac{6.6}{L}\right)^4, \quad (1)$$

where n_e is the electron density in cm^{-3}.

Key plume parameters are determined, such as the maximum electron density (N_{e_max}), the average electron density (N_{e_mean}), ΔL and ΔMLT. ΔMLT is defined as difference between the MLT of the entrance and exit of the plume. N_{e_max} is defined as the peak value of electron density during a plume crossing, while N_{e_mean} refers to the mean value of electron density over the en-

tire crossing interval. For the event shown in Figure 1, N_{e_max} is 100.8 cm^{-3}, N_{e_mean} is 59.2 cm^{-3}, ΔL is 0.5 and ΔMLT is 0.19.

2 Statistical Analysis

2.1 Spatial Distribution

We analyze data from THEMIS-A and THEMIS-E spacecraft over the period from 1 January 2011 to 31 December 2022, during which full coverage in both MLT and L across the entire magnetosphere was achieved. Based on the identification criteria of plume events described above, a total of 488 detached plume events is identified, including 159 events observed by THEMIS-A and 329 events by THEMIS-E.

Figure 2 shows the locations of the spacecraft trajectories associated with all identified plume events, projected onto the GSE XY plane. Each short line segment represents the portion of the spacecraft trajectory during a plume crossing. The color of each segment indicates the electron density of the plume. The geosynchronous orbit is marked by a dotted line for reference. The spatial distribution of plume crossings exhibits a pronounced dawn-dusk asymmetry that more events occur in the dusk sector, while only a few are observed in the dawn sector. Some plumes are observed at high L, especially near the dusk sector.

To further reveal the statistical characteristics of plume events, Figure 3 provides a quantitative analysis of the plume distribution shown in Figure 2. Figure 3(a) (b) summarize the number of plume events versus L and MLT, respectively. Plume events are concentrated between L = 5 and 8.5, peaking at L = 6 – 6.5, with a mean L of 6.56. Besides, events concentrate in 14 – 22 MLT, with the highest occurrence in 16 – 18 MLT, which also shows that plumes preferentially occur in the dusk sector of the magnetosphere.

To investigate whether plume characteristics exhibit systematic variations across different MLT sectors, we group the events into four commonly used MLT sectors: dawnside (3 – 9 MLT), dayside (9 – 15 MLT), duskside (15 – 21 MLT), and nightside (21 – 3 MLT). Figure 4

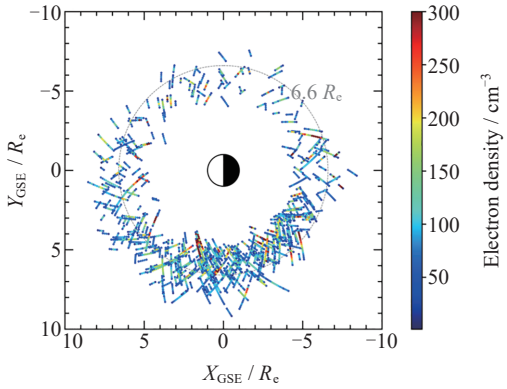


Fig. 2 Locations of plasmaspheric plume events observed by the THEMIS-A and THEMIS-E spacecraft from 2011 to 2022, projected onto the GSE XY plane. Each short line segment represents a portion of the spacecraft orbit during a plume crossing. Electron density is indicated by color. The geosynchronous orbit is indicated by a dashed circle

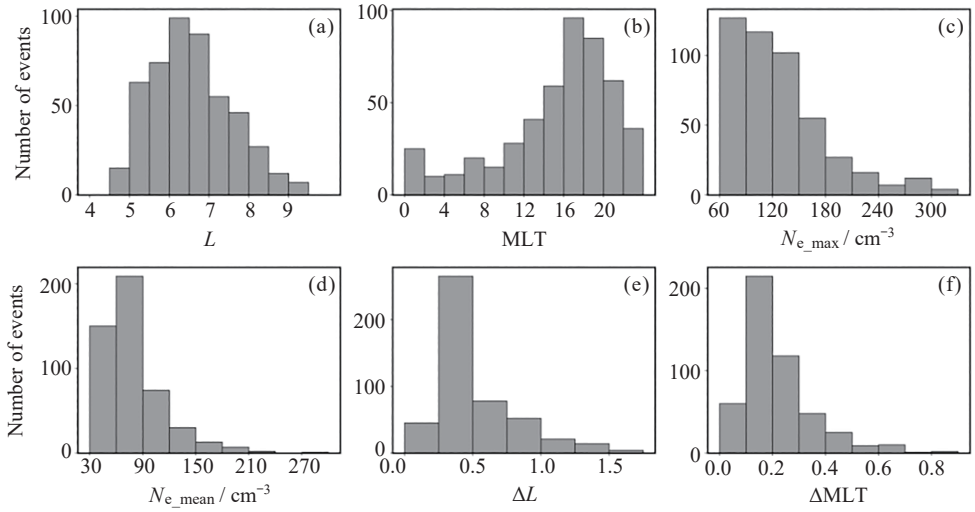


Fig. 3 Number of plasmaspheric plume events as functions of L, MLT, N_{e_max}, N_{e_mean}, ΔL, ΔMLT

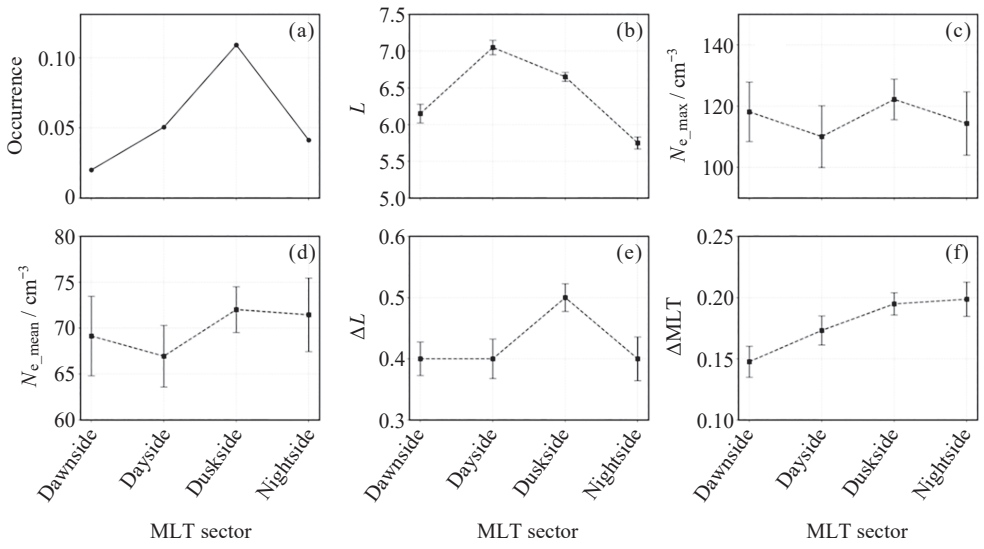


Fig. 4 Occurrence rate of plume events in the four MLT sectors (a). Median values of L, N_{e_max}, N_{e_mean}, ΔL, ΔMLT for plume events in each MLT sector

Table 1 Characteristics of plasmaspheric plumes

Name	**Symbol**	**Mean value**	**Median value**
Magnetic Local Time	MLT	15.34	16.84
Radial distance	L	6.56	6.45
Radial width	ΔL	0.56	0.40
Peak electron density	N_{e_max}	144.26 cm^{-3}	120.32 cm^{-3}
Mean electron density	N_{e_mean}	81.34 cm^{-3}	70.95 cm^{-3}

compares plume properties across these four sectors. To mitigate orbital sampling bias, we record each MLT sector in which the spacecraft crossed outward through L = 7. The occurrence rate for each sector (Figure 4a) is computed as the number of plume crossings normalized by the number of corresponding orbital segments. The results shown in Figure 2, 3(b) and 4(a) consistently indicate that plume occurrence is significantly higher on the duskside than that on the dawnside, in agreement with previous observations[6,40–43,62–64].

Figure 4(b) shows that plumes on the dayside reach larger L than those in other sectors, while plumes on the nightside have the lowest L. This distribution is consistent with the expected rotation and outward transport of plume structures. Plumes originating near the duskside move radially outward under enhanced convection and progressively wrap sunward toward the noon sector. As a result, plume crossings on the dayside are observed at larger L, in agreement with particle-tracing simulations[65].

2.2 Electron Density Characteristics

Figure 3(c) shows the distribution of plume events as a function of N_{e_max}. Most events have N_{e_max} < 180 cm^{-3}, with a peak in the 60 – 90 cm^{-3} range. The average value of N_{e_max} across all identified events is 144.26 cm^{-3}. Figure 3d presents the distribution of plume events as a function of N_{e_mean}, which also peaks at 60 – 90 cm^{-3}, with most values below 120 cm^{-3}. The overall mean N_{e_mean} is 81.34 cm^{-3}. These results indicate that the majority of plume events typically concentrated in the 60 – 90 cm^{-3} range. Moreover, plume electron densities exhibit clear MLT dependence. From Figure 4(c) (d), we find that duskside plumes have the highest electron densities, with N_{e_max} around 122 cm^{-3} and N_{e_mean} near 72 cm^{-3}.

Having described the statistical distributions of plume electron densities across MLT sectors, further insight into their spatial characteristics as a function of L is

provided in Figure 5. Figure 5(a)(c) show scatter plots of individual plume events for N_{e_max} and N_{e_mean}, respectively. The corresponding median distributions of Figure 5(a) (c) are shown in Figure 5(b)(d), providing a more robust representation of the underlying trends. Both N_{e_mean} and N_{e_max} peak around L = 5 – 6 and decrease toward larger L, suggesting that the densest plumes occur near Earth and become progressively diluted as they extend outward.

The density variation within the plumes is an important factor influencing wave generation and particle precipitation[35]. We quantify the density gradients of each plasmaspheric plume. For a given plume, L_{min} and L_{max} denote the minimum and maximum L sampled, with corresponding electron densities N_e (L_{min}) and N_e (L_{max}), respectively. L_{peak} represents the L at which the electron density reaches its maximum. The positive gradient is defined as

$$G_{pos} = \frac{N_{e_max} - Ne\,(L_{min})}{L_{peak} - L_{min}}. \tag{2}$$

The negative gradient is defined as

$$G_{neg} = \left| \frac{Ne\,(L_{max}) - N_{e_max}}{L_{max} - L_{peak}} \right|. \tag{3}$$

Figure 6 shows the distributions of G_{pos} (Figure 6a) and G_{neg} (Figure 6b) associated with plasmaspheric

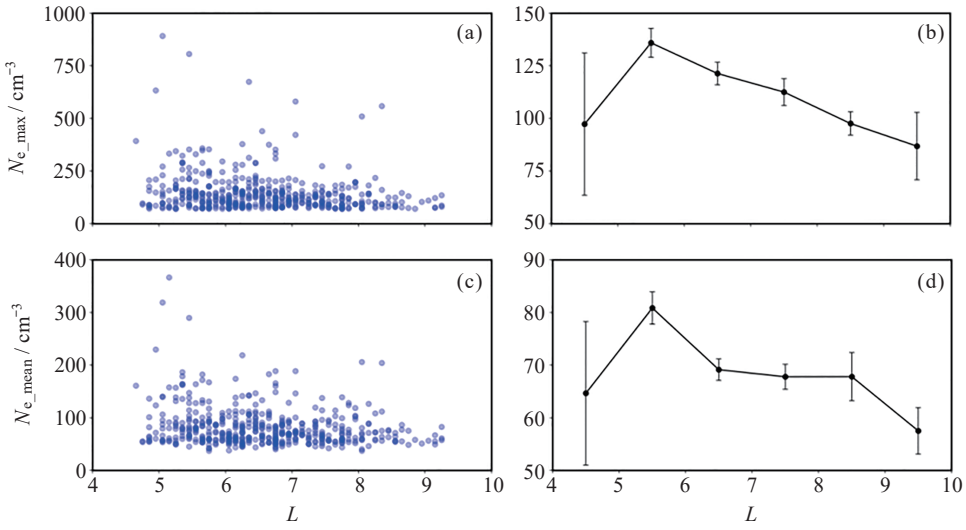


Fig. 5 Scatter plots of N_{e_max} (a) and N_{e_mean} (c) versus L for all plume events, and the corresponding median values of N_{e_max} (b) and N_{e_mean} (d) as a function of L

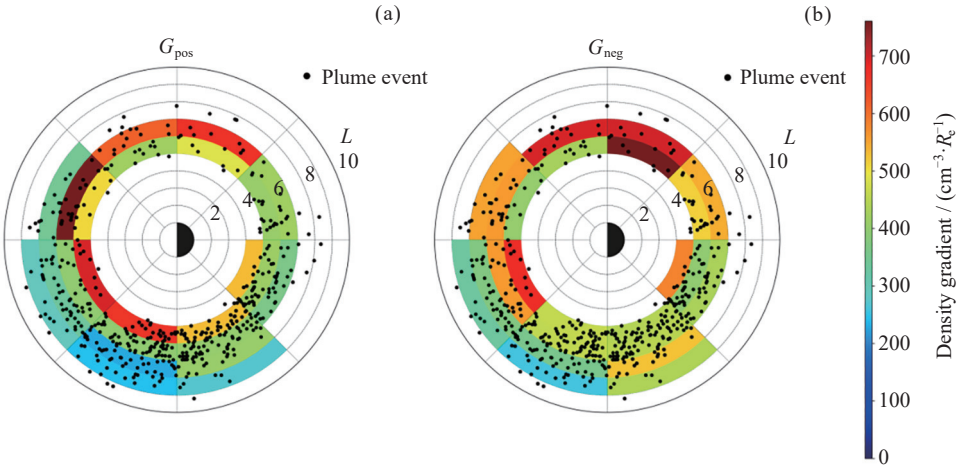


Fig. 6 Electron density gradients of plasmaspheric plumes in MLT-L coordinates. (a) Mean value of G_{pos}. (b) Mean value of G_{neg}. Black dots indicate plume event locations

plumes in MLT-L coordinates. Each dot marks a single plume event, and the color of each bin encodes the mean magnitude of the density gradient. Bins containing fewer than five events are removed to avoid low-sample bias. Both G_{pos} and G_{neg} generally decrease with increasing L and exhibit a clear dawn-dusk asymmetry, with steeper gradients on the dawnside and weaker gradients on the duskside for $L > 6$.

The systematic decrease of both positive and negative density gradients with increasing L suggests that plume structures become progressively more diffuse as they extend outward, consistent with plasma dilution during sunward transport. In addition, the pronounced dawn-dusk asymmetry indicates that plume boundary sharpness depends on MLT. This asymmetry may reflect differences in plume age, convection strength, and transport history across MLT sectors. Notably, G_{pos} also appear large in the 12 – 18 MLT sector at $L = 4 – 5$.

These results are relevant to the mechanisms suggested by previous studies, such as Zhou *et al.*[35], who proposed that sharp plasma density variations near plume edges could drive dispersed precipitation events, and numerical simulations showing that three-dimensional field line resonances preferentially develop at duskside plume boundaries where gradients are strongest[66]. The distribution presented here may help guide future efforts to assess the roles of plume gradients in broader magnetospheric dynamics.

2.3 Morphological Properties of Plasmaspheric Plumes

The morphological characteristics of plasmaspheric plumes are crucial for understanding the mechanisms underlying plume formation and evolution. Figure 3(e) shows the distribution of plume events as a function of ΔL. Most plumes exhibit ΔL between 0.2 and 1.0, with the highest number of events occurring within the 0.25 – 0.5. Figure 3(f) shows the distribution of plume events as a function of ΔMLT. Most plumes exhibit ΔMLT < 0.4, with the highest number of events occurring within the range of 0.1 – 0.2 MLT. These distributions suggest that the majority of plumes are relatively narrow both in ΔL and ΔMLT.

The morphological characteristics of plasmaspheric plumes vary with MLT. From Figure 4(e), the ΔL of plasmaspheric plumes is larger on the duskside compared to the other MLT sectors. In Figure 4(f), ΔMLT progressively decreases from the nightside through the duskside and dayside to the dawnside sector, indicating a gradual narrowing of plume structures toward the dawnside. This feature is consistent with plume structures extending and trailing sunward from the duskside under the combined effects of corotation and convection [18,22,24,67].

To better understand the structure of a plasmaspheric plume, we examine how electron density of plume varies with ΔL in Figure 7. Both N_{e_max} (Figure 7a) and N_{e_mean} (Figure 7b) exhibit a positive correlation with ΔL, which can be explained by the fact that regions closer to the tip of the plume are narrower and have lower density. Besides, Goldstein and Sandel[67] found that the plume narrows after plasma is steadily eroded *via* sunward motion driven by the enhanced convection. Borovsky and Denton[52] found that plume plasma densi-

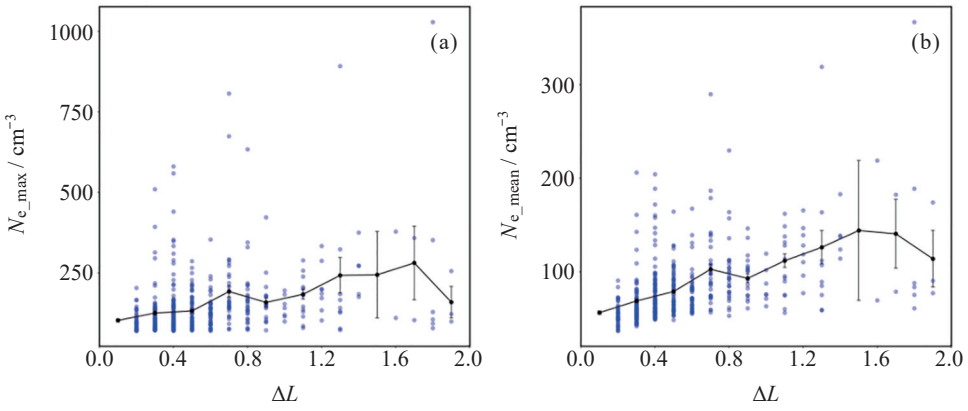


Fig. 7 Distributions of plume electron densities. (a) N_{e_max} and (b) N_{e_mean} are as a function of ΔL. Each dot represents a single plume event

ty and ΔL tends to decrease with the age of the plume. Based on their observations, our results further suggest that plume electron density decreases more rapidly than ΔL during plume evolution.

We compare the mean MLT of the plume crossings identified in this study with previous observations at geosynchronous orbit (~ 15 h) reported by Borovsky and Denton [52]. The average MLT obtained in this study (15.34 h) is very close to their reported value, providing an independent consistency check and supporting the reliability of our statistical results. In order to distinguish events occurring near geosynchronous orbit from those near the magnetosphere, we divide the events into two groups based on L: those located inside and outside L=7, as shown in Figure 8a and 8b, respectively. The most probable MLT position of plumes shifts from 17.5 h at $L \leqslant 7$ to 15.3 h at $L > 7$, exhibiting a dusk-to-prenoon displacement similar to that a displacement toward the prenoon sector reported by Walsh *et al.*[6].

3 Conclusions

A comprehensive survey of 488 detached plasmaspheric plumes based on THEMIS measurements shows that plumes occur predominantly at L = 5 – 8.5, with a peak at L = 6 – 6.5. The highest occurrence is found in 14 – 22 MLT, with rates reaching ~13% in 16 – 18 MLT. In addition, plumes on the dayside reach higher L values than those in other sectors, indicating a sunward-wrapping outward extension from the duskside.

The electron densities of plumes typically concentrate in the range of 60 – 90 cm^{-3}. Both $N_{\mathrm{e_mean}}$ and $N_{\mathrm{e_max}}$ peak near L = 5 – 6 and decrease outward, indicating that plumes become progressively diluted as they extend outward. Among the four MLT sectors, plumes on the duskside exhibit the largest occurrence rates, electron densities, and ΔL. Both G_{pos} and G_{neg} generally decrease with increasing L and exhibit a clear dawn-dusk asymmetry, with steeper gradients on the dawnside and weaker gradients on the duskside for $L > 6$.

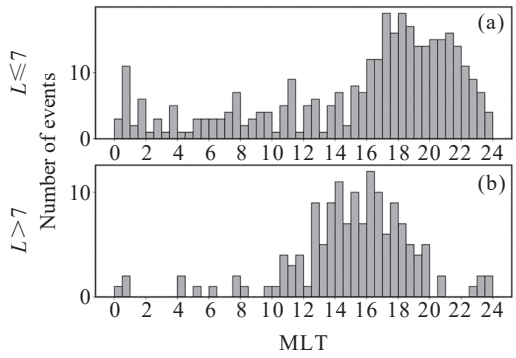


Fig. 8 MLT distribution of plasmaspheric plumes at $L \leqslant 7$ (a) and at $L > 7$ (b)

Morphologically, most plumes have ΔL between 0.2 and 1.0. Plume density increases with ΔL, implying that the electron density of plumes decreases more rapidly than ΔL during plume evolution. In addition, the most probable MLT of plume exhibits a dusk-to-prenoon displacement.

These results provide a comprehensive characterization of the spatial, density, and morphological properties of detached plasmaspheric plumes across the magnetosphere, offering quantitative constraints that can guide future investigations of plume formation, transport, and their influence on magnetospheric dynamics. The results may also provide essential inputs for improving global magnetospheric models, particularly those involving mass loading, convection dynamics, and wave-particle interactions.

Acknowledgment We acknowledge V Angelopoulos for use of data from the THEMIS Mission, J W Bonnell and F S Mozer for use of EFI data, and C W Carlson and J P McFadden for use of ESA data.

Ethical Approval This article does not contain any studies with human participants or animals performed by any of the authors.

Conflict of Interests The authors declare that there is no conflict of interests.

References

[1] CARPENTER D L. Whistler evidence of a 'knee' in the magnetospheric ionization density profile[J]. *Journal of Geophysical Research*, 1963, **68**(6): 1675-1682

[2] CARPENTER D L. Whistler studies of the plasmapause in the magnetosphere: 1. Temporal variations in the position of the knee and some evidence on plasma motions near the knee[J]. *Journal of Geophysical Research*, 1966, **71**(3): 693-709

[3] LEMAIRE J F, GRINGAUZ K I, CARPENTER D L, *et al*. The Earth's Plasmasphere[M]. Cambridge: Cambridge University Press, 1998

[4] DARROUZET F, DE KEYSER J, PIERRARD V. The Earth's Plasmasphere: A CLUSTER and IMAGE Perspective[M]. New York: Springer, 2009

[5] GALVAN D A, MOLDWIN M B, SANDEL B R, *et al*. On the causes of plasmaspheric rotation variability: IMAGE EUV observations[J]. *Journal of Geophysical Research*: *Space Physics*, 2010, **115**(A1): A01214

[6] WALSH B M, SIBECK D G, NISHIMURA Y, *et al*. Statistical analysis of the plasmaspheric plume at the magnetopause[J]. *Journal of Geophysical Research*: *Space Physics*, 2013, **118**(8): 4844-4851

[7] LIU X, LIU W, CAO J B, *et al*. Dynamic plasmapause model based on THEMIS measurements[J]. *Journal of Geophysical Research*: *Space Physics*, 2015, **120**(12): 10543-10556

[8] GALLAGHER D L, COMFORT R H, KATUS R M, *et al*. The breathing plasmasphere: erosion and refilling[J]. *Journal of Geophysical Research*: *Space Physics*, 2021, **126**(4): e2020JA028727

[9] RIPOLL J F, PIERRARD V, CUNNINGHAM G S, *et al*. Modeling of the cold electron plasma density for radiation belt physics[J]. *Frontiers in Astronomy and Space Sciences*, 2023, **10**: 1096595

[10] LÜ Jingtian, ZHANG Xiaoxin, HE Fei, *et al*. State studies of Earth's plasmasphere[J]. *Reviews of Geophysics and Planetary Physics*, 2023, **54**(4): 417-433 (吕景天, 张效信, 何飞, 等. 地球等离子体层研究进展 [J]. 地球与行星物理论评 (中英文), 2023, **54**(4): 417-433)

[11] BRICE N M. Bulk motion of the magnetosphere[J]. *Journal of Geophysical Research*, 1967, **72**(21): 5193-5211

[12] HORVATH I, LOVELL B C. Outer-plasmasphere plasma hole scenarios promoting hot zone and sub-auroral polarization streams (SAPS) E field development[J]. *Journal of Geophysical Research*: *Space Physics*, 2025, **130**(5): e2024JA033184

[13] XIAO Z, YU S M, SHI H, *et al*. A brief of recent research progress on ionospheric disturbances[J]. *Science China Information Sciences*, 2013, **56**(12): 1-9

[14] XIAO Zuo, LIU Kaijun, ZHANG Donghe. Some typical records of ionospheric doppler shift and their significance in the study of ionospheric morphology[J]. *Chinese Journal of Space Science*, 2002, **22**(4): 321-329 (肖佐, 刘凯军, 张东和. 典型电离层多普勒记录及其讨论 [J]. 空间科学学报, 2002, **22**(4): 321-329)

[15] XIAO Zuo, XIE Hong. Equatorial Spread-F initiated by acoustic-gravity waves[J]. *Chinese Journal of Space Science*, 1994, **14**(3): 183-190 (肖佐, 谢红. 声重波激发的赤道 Spread-F 不稳定性 [J]. 空间科学学报, 1994, **14**(3): 183-190)

[16] CARPENTER D L, ANDERSON R R. An ISEE/whistler model of equatorial electron density in the magnetosphere[J]. *Journal of Geophysical Research*: *Space Physics*, 1992, **97**(A2): 1097-1108

[17] CARPENTER D L, LEMAIRE J. The plasmasphere boundary layer[J]. *Annales Geophysicae*, 2004, **22**(12): 4291-4298

[18] CHEN A J, WOLF R A. Effects on the plasmasphere of a time-varying convection electric field[J]. *Planetary and Space Science*, 1972, **20**(4): 483-509

[19] LEMAIRE J F. The formation plasmaspheric tails[J]. *Physics and Chemistry of the Earth, Part C*: *Solar, Terrestrial & Planetary Science*, 2000, **25**(1/2): 9-17

[20] MOLDWIN M B, DOWNWARD L, RASSOUL H K, *et al*. A new model of the location of the plasmapause: CRRES results[J]. *Journal of Geophysical Research*: *Space Physics*, 2002, **107**(A11): 1339

[21] GOLDSTEIN J, DE PASCUALE S, KLETZING C, *et al*. Simulation of van allen probes plasmapause encounters[J]. *Journal of Geophysical Research*: *Space Physics*, 2014, **119**(9): 7464-7484

[22] GREBOWSKY J M. Model study of plasmapause motion[J]. *Journal of Geophysical Research*, 1970, **75**(22): 4329-4333

[23] CHEN A J, GREBOWSKY J M. Plasma tail interpretations of pronounced detached plasma regions measured by Ogo 5[J]. *Journal of Geophysical Research*, 1974, **79**(25): 3851-3855

[24] LU Z Y, LI J C, ZHANG S, *et al*. Statistical properties of Pc4-5 ULF waves in plasmaspheric plumes[J]. *Geophysical Research Letters*, 2024, **51**(6): e2023GL107514

[25] YUAN Z G, DENG X H, LIN X, *et al*. Link between EMIC waves in a plasmaspheric plume and a detached sub-auroral proton arc with observations of cluster and IMAGE satellites[J]. *Geophysical Research Letters*, 2010, **37**(7): L07108

[26] CHEN L J, THORNE R M, LI W, *et al*. Modulation of plasmaspheric hiss intensity by thermal plasma density structure[J]. *Geophysical Research Letters*, 2012, **39**(14): L14103

[27] HALFORD A J, FRASER B J, MORLEY S K. EMIC waves and plasmaspheric and plume density: CRRES results[J]. *Journal of Geophysical Research*: *Space Physics*, 2015, **120**(3): 1974-1992

[28] GRISON B, HANZELKA M, BREUILLARD H, *et al*. Plasmaspheric plumes and EMIC rising tone emissions[J]. *Journal of Geophysical Research*: *Space Physics*, 2018, **123**(11): 9443-9452

[29] KIM K C, SHPRITS Y. Statistical analysis of hiss waves in plasmaspheric plumes using van allen probe observations[J]. *Journal of Geophysical Research*: *Space Physics*, 2019, **124**(3): 1904-1915

[30] HE B, ZHANG D J, LIU W L, *et al*. Statistical study on coherent quasi-periodic emissions based on multi-satellite measurements[J]. *Journal of Geophysical Research*: *Space Physics*, 2025, **130**(5): e2025JA033890

[31] SUMMERS D, NI B B, MEREDITH N P, *et al*. Electron scattering by whistler-mode ELF hiss in plasmaspheric plumes[J]. *Journal of Geophysical Research*: *Space Physics*, 2008, **113**(A4): A04219

[32] ZONG Q G, REN J, ZHOU X Z. Interactions between ULF waves and cold plasmaspheric particles[M]//ZONG Q G, ESCOUBET P, SIBECK D, *et al*. Dayside Magnetosphere Inter-

actions. Hoboken: American Geophysical Union, 2020: 265-284

[33] SPASOJEVIC M, FUSELIER S A. Temporal evolution of proton precipitation associated with the plasmaspheric plume[J]. *Journal of Geophysical Research: Space Physics*, 2009, **114**(A12): A12201

[34] YUAN Z G, LI M, XIONG Y, *et al*. Simultaneous observations of precipitating radiation belt electrons and ring current ions associated with the plasmaspheric plume[J]. *Journal of Geophysical Research: Space Physics*, 2013, **118**(7): 4391-4399

[35] ZHOU R X, ZHANG X J, ARTEMYEV A V, *et al*. Characteristics of energy-latitude dispersed electron precipitation driven by EMIC waves[J]. *Journal of Geophysical Research: Space Physics*, 2025, **130**(4): e2024JA033501

[36] BOROVSKY J E, DENTON M H. Effect of plasmaspheric drainage plumes on solar-wind/magnetosphere coupling[J]. *Geophysical Research Letters*, 2006, **33**(20): L20101

[37] BOROVSKY J E, DENTON M H, DENTON R E, *et al*. Estimating the effects of ionospheric plasma on solar wind/magnetosphere coupling via mass loading of dayside reconnection: ion-plasma-sheet oxygen, plasmaspheric drainage plumes, and the plasma cloak[J]. *Journal of Geophysical Research: Space Physics*, 2013, **118**(9): 5695-5719

[38] WALSH B M, FOSTER J C, ERICKSON P J, *et al*. Simultaneous ground- and space-based observations of the plasmaspheric plume and reconnection[J]. *Science*, 2014, **343**(6175): 1122-1125

[39] DE KEYSER J, CARPENTER D L, DARROUZET F, *et al*. CLUSTER and IMAGE: new ways to study the earth's plasmasphere[J]. *Space Science Reviews*, 2009, **145**(1/2): 7-53

[40] LEE S H, ZHANG H, ZONG Q G, *et al*. A statistical study of plasmaspheric plumes and ionospheric outflows observed at the dayside magnetopause[J]. *Journal of Geophysical Research: Space Physics*, 2016, **121**(1): 492-506

[41] LI H M, FU T X, TANG R X, *et al*. Statistical study and corresponding evolution of plasmaspheric plumes under different levels of geomagnetic storms[J]. *Annales Geophysicae*, 2022, **40**(2): 167-177

[42] YANG Z R, LI H M, YUAN Z G, *et al*. Width of plasmaspheric plumes related to the level of geomagnetic storm intensity[J]. *Annales Geophysicae*, 2022, **40**(6): 673-685

[43] DARROUZET F, DE KEYSER J, DÉCRÉAU P M E, *et al*. Statistical analysis of plasmaspheric plumes with cluster/WHISPER observations[J]. *Annales Geophysicae*, 2008, **26**(8): 2403-2417

[44] FOSTER J C, ERICKSON P J, COSTER A J, *et al*. Ionospheric signatures of plasmaspheric tails[J]. *Geophysical Research Letters*, 2002, **29**(13): 1623

[45] SINGH A K, SINGH R P, SIINGH D. State studies of earth's plasmasphere: a review[J]. *Planetary and Space Science*, 2011, **59**(9): 810-834

[46] XIANG T Y, REN J, ZONG Q G, *et al*. Periodic density structures around the plasmaspheric plume boundary and their association with ULF waves[J]. *Journal of Geophysical Research: Space Physics*, 2025, **130**(6): e2025JA034044

[47] DENT Z C, MANN I R, MENK F W, *et al*. A coordinated ground-based and IMAGE satellite study of quiet-time plasmaspheric density profiles[J]. *Geophysical Research Letters*, 2003, **30**(12): 1600

[48] SU Y J, THOMSEN M F, BOROVSKY J E, *et al*. A linkage between polar patches and plasmaspheric drainage plumes[J]. *Geophysical Research Letters*, 2001, **28**(1): 111-113

[49] GARCIA L N, FUNG S F, GREEN J L, *et al*. Observations of the latitudinal structure of plasmaspheric convection plumes by IMAGE-RPI and EUV[J]. *Journal of Geophysical Research: Space Physics*, 2003, **108**(A8): 1321

[50] DARGENT J, AUNAI N, LAVRAUD B, *et al*. Simulation of plasmaspheric plume impact on dayside magnetic reconnection[J]. *Geophysical Research Letters*, 2020, **47**(4): e2019GL086546

[51] MOLDWIN M B, HOWARD J, SANNY J, *et al*. Plasmaspheric plumes: CRRES observations of enhanced density beyond the plasmapause[J]. *Journal of Geophysical Research: Space Physics*, 2004, **109**(A5): A05202

[52] BOROVSKY J E, DENTON M H. A statistical look at plasmaspheric drainage plumes[J]. *Journal of Geophysical Research: Space Physics*, 2008, **113**(A9): A09221

[53] ANGELOPOULOS V. The THEMIS mission[J]. *Space Science Reviews*, 2008, **141**(1): 5-34

[54] BONNELL J W, MOZER F S, DELORY G T, *et al*. The electric field instrument (EFI) for THEMIS[J]. *Space Science Reviews*, 2008, **141**(1/2/3/4): 303-341

[55] MCFADDEN J P, CARLSON C W, LARSON D, *et al*. The THEMIS ESA plasma instrument and in-flight calibration[J]. *Space Science Reviews*, 2008, **141**(1/2/3/4): 277-302

[56] MOZER F S. Analyses of techniques for measuring DC and AC electric fields in the magnetosphere[J]. *Space Science Reviews*, 1973, **14**(2): 272-313

[57] PEDERSEN A, LYBEKK B, ANDRÉ M, *et al*. Electron density estimations derived from spacecraft potential measurements on cluster in tenuous plasma regions[J]. *Journal of Geophysical Research: Space Physics*, 2008, **113**(A7): A07S33

[58] LI W, THORNE R M, NISHIMURA Y, *et al*. THEMIS analysis of observed equatorial electron distributions responsible for the chorus excitation[J]. *Journal of Geophysical Research: Space Physics*, 2010, **115**(A6): A00F11

[59] NISHIMURA Y, BORTNIK J, LI W, *et al*. Structures of dayside whistler-mode waves deduced from conjugate diffuse aurora[J]. *Journal of Geophysical Research: Space Physics*, 2013, **118**(2): 664-673

[60] SHEELEY B W, MOLDWIN M B, RASSOUL H K, *et al*. An empirical plasmasphere and trough density model: CRRES ob-

servations[J]. *Journal of Geophysical Research*: *Space Physics*, 2001, **106**(A11): 25631-25641

[61] ZHANG W X, NI B B, HUANG H, *et al*. Statistical properties of hiss in plasmaspheric plumes and associated scattering losses of radiation belt electrons[J]. *Geophysical Research Letters*, 2019, **46**(11): 5670-5680

[62] CHEN S H, MOORE T E. Magnetospheric convection and thermal ions in the dayside outer magnetosphere[J]. *Journal of Geophysical Research*: *Space Physics*, 2006, **111**(A3): A03215

[63] GOLDSTEIN J, SANDEL B R, THOMSEN M F, *et al*. Simultaneous remote sensing and in situ observations of plasmaspheric drainage plumes[J]. *Journal of Geophysical Research*: *Space Physics*, 2004, **109**(A3): A03202

[64] KIM K H, GOLDSTEIN J, BERUBE D. Plasmaspheric drainage plume observed by the polar satellite in the prenoon sector and the IMAGE satellite during the magnetic storm of 11 April 2001[J]. *Journal of Geophysical Research*: *Space Physics*, 2007, **112**(A6): A06237

[65] MOORE T E, FOK M C, DELCOURT D C, *et al*. Plasma plume circulation and impact in an MHD substorm[J]. *Journal of Geophysical Research*: *Space Physics*, 2008, **113**(A6): A06219

[66] ELSDEN T, WRIGHT A N. Polarization properties of 3-D field line resonances[J]. *Journal of Geophysical Research*: *Space Physics*, 2022, **127**(2): e2021JA030080

[67] GOLDSTEIN J, SANDEL B R. The global pattern of evolution of plasmaspheric drainage plumes[M]//BURCH J, SCHULZ M, SPENCE H. Geophysical Monograph Series. Washington: American Geophysical Union, 2005: 1-22

Author Biography



HU Yuanqiao Female, born in Chengdu, Sichuan in May 2002. She is a student at School of Space and Earth Sciences of Beihang University. She mainly focuses on research in plasmasphere and plasmaspheric density structures.
E-mail: yuanqiaohu@buaa.edu.cn



LIU Wenlong（Corresponding author） Male, born in Weihai, Shandong in November 1980. He is a professor at School of Space and Earth Sciences of Beihang University. He mainly focuses on the research of the dynamic processes in the Earth's magnetosphere.
E-mail: liuwenlong@buaa.edu.cn



YAN Li（Corresponding author） Female, born in Xuancheng, Anhui in October 2000. She is a student at the School of Space and Earth Sciences of Beihang University. She mainly focuses on the dynamics of the Earth's magnetosphere and magnetosphere-ionosphere coupling.
E-mail: yanli1@buaa.edu.cn